Available online at www.sciencedirect.com

ScienceDirect

Procedia CIRP 131 (2025) 19–25

www.elsevier.com/locate/procedia

3rd CIRP Conference on Composite Material Parts Manufacturing

Modeling of temperature fields in milling of unidirectionally reinforced CFRP depending on the fibre orientation angle and the effective width of cut

Wolfgang Hintze[a], Ganna Shchegel[a,*], Jan Mehnen[a], Carsten Möller[a], Jan Dege[a]

[a]*Institute of Production Management and Technology, Hamburg University of Technology, Denickestraße 17, Hamburg 21073, Germany*

* Corresponding author. Tel.: +49-4042-878-4192. *E-mail address:* ganna.shchegel@tuhh.de

Abstract

CFRP parts are conventionally used within various industries; however, during machining these components, the generated heat is a very relevant limiting factor. Exceeding the glass transition temperature can lead to workpiece degradation, reduced strength, and shorter lifetime. During up-cut milling of unidirectional (UD) CFRP with PCD cutters, the temperature was measured using thermocouples and a thermographic camera, while the cutting torque was measured with a rotating dynamometer. The maximum temperature increase at the machined surface, the heat flow from the machining zone into the material, and the ratio of heat flow to cutting power were simulated. An analytical model developed earlier for the temperature field in machining orthotropic composites with arbitrary fibre orientation was used. The results indicate that cutting power, heat flow, and the ratio of heat flow to cutting power exhibit approximate symmetry relative to the fibre orientation angle $\Phi = 90°$. Introducing the concept of the fibre orientation symmetry angle is useful. Unexpected fractures of larger segments of remaining UD CFRP material occur at all feeds at higher fibre orientation and engagement angles within a small range of fibre cutting angles near 45°, significantly reducing the nominal width of cut and impairing results. The effective width of cut was evaluated based on the drop in cutting torque, measured at various fibre orientation angles, cutting speeds, feeds, and nominal widths of cut. The highest maximum temperature increase consistently occurs at $\Phi = 135°$. As an overall effect, higher cutting speeds lead to increased cutting power, heat flow, and maximum temperature at the machined surface, but result in a smaller depth of the heat-affected zone. The simulations conclude that a higher fibre orientation symmetry angle leads to a higher equivalent heat flux, shorter thermal contact length, and reduced heat flow, and vice versa. In the future, the influence of different tools and composite materials needs to be investigated.

Keywords: CFRP; Milling; Moving Heat Source; Surface Damage; Temperature; Heat Flow; Fibre Orientation Angle

1. Introduction and state of the art

Due to their mechanical, thermal, and chemical properties, carbon fibre reinforced plastics (CFRP) are widely used in the aerospace and automotive industries, as well as in medical technology and sports. To maximize the mechanical properties of fibre reinforced plastics (FRP), the fibres are aligned to form unidirectional (UD) composite layers. After autoclave hardening, the outline contour of the formed lightweight structures is trimmed in milling to achieve dimensional accuracy [1]. During machining, the maximum permissible temperatures for the matrix, particularly the glass transition temperature, can be exceeded in the machining zone [2]. This can lead to component damage, failure, and unreliable mechanical characteristics. Because machining is performed at the end of the value chain for components that are usually very complex to produce, there are high demands on the quality and reliability of the process.

The value of the maximum temperature change ΔT_{max} and the steepness of its spatial distribution determine the size of the heat-affected zone and are highly dependent on the processing parameters, tools used, and material properties. To achieve an

10.1016/j.procir.2024.09.006

optimal machining process without exceeding the critical temperatures, a profound understanding of these underlying dependencies is essential.

Nomenclature

$a_{e,eff}$	effective width of cut
$a_{e,nom}$	nominal width of cut
a_p	depth of cut
C_p	specific heat capacity
d_t	tool diameter
f	feed
h	chip thickness
K_0	modified Bessel function of the second kind of order zero
k_{11}	thermal conductivity in 1st orthotropic direction parallel to fibres
k_{33}	thermal conductivity in 2nd orthotropic direction perpendicular to fibres
n	number of spindle revolutions
l_m	length of machined path
P_c	cutting power
P_{HS}	heat flow into the workpiece
q_{HS}	heat flux of the heat source
r_β	radius of the tool cutting-edge
R_W	ratio of the heat flow from the heat source into the workpiece to the cutting power
S	integration variable
s_{HS}	thermal contact length of the heat source
t	thickness of the tested CFRP-panels
$T_{MSS,\Phi,SS}$	temperature distribution due to action of a moving strip source (MSS) in steady state (SS)
T_g	glass transition temperature
v_c	cutting speed
v_f	feed rate and heat source velocity
x_{HS}	horizontal position of the centre of the heat source
x_n	horizontal coordinate of the point of interest for which the temperature is modeled
z	distance from the machined surface to the thermographic camera measurement line
z_n	vertical coordinate of the point of interest for which the temperature is modeled
ΔT_{max}	maximum temperature change
ζ_Φ	fibre orientation symmetry angle
θ	fibre cutting angle
ρ_w	density
Φ	fibre orientation angle
φ	engagement angle

Unlike many other fibre types, carbon fibres have much higher thermal conductivity compared to the matrices typically used in FRP [3]. This results in significant differences in thermal distribution along the orthotropic directions, both parallel and perpendicular to the dominant reinforcement fibre orientation [4]. Consequently, there are considerable variations in the maximum temperature changes ΔT_{max}, depending on the fibre orientation angle Φ. The angle Φ is defined as the angle between the feed rate vector v_f and the fibre direction on the bulk side of the trimmed panel (as opposed to its cut-off side) [5].

Furthermore, the feed f and feed rate v_f directly influence the chip thickness h for each fibre cutting angle θ, where θ is defined as the angle between the cutting speed vector v_c and the fibre direction [4]. The cutting speed v_c and the number of revolutions n significantly affect the dynamic behavior of the FRP [2]. The corresponding values of cutting forces and moments determine the cutting temperature achieved [3].

The potential increase in temperature is directly related to the heat flow into the workpiece P_{HS}. According to numerical studies [6], this heat flow is highly dependent on the type of cutter used. Heat conduction from the tool contact is considered the dominant factor in the heat flow into the workpiece, leading to its temperature increase [7]. Jaeger's analytical heat conduction model [8] has been used several times to calculate temperatures for machining thermally isotropic materials. In [9], this analytical model was significantly improved by adapting it for orthotropic materials with arbitrary fibre orientation angles. The heat source is modeled as a moving strip source in a steady state [10]. Additionally, the ratio R_W of the heat flow into the workpiece P_{HS} to the cutting power P_c was studied in [6].

Despite existing research, there remains a gap in understanding the temperature field T in the edge zone of unidirectional CFRP resulting from various fibre orientation angles Φ under different machining conditions. Consequently, a reliable method for assessing thermal edge zone damage in milling of UD-CFRP and related high-performance FRPs based on experimentally determined thermal parameters, is still lacking. To address this, this study proposes to determine the thermal parameters of the machining process empirically through testing using a physically based analytical model [9]. Their dependence on the processing conditions is also investigated in this study.

2. Materials and methods

Side milling experiments were conducted on UD-CFRP panels with varying fibre orientations to facilitate subsequent simulations of the temperature fields. Temperatures were measured at four distances from the cutting surface using thermocouples and a thermographic camera.

2.1. Tools and material

Work-sharp double-edged polycrystalline diamond (PCD) cutters were used for the experiments, which were conducted using up-cut milling in accordance with industrial practice. The parameters of the tool are listed in Table 1.

Table 1. Geometry of the double-edged polycrystalline diamond peripheral milling tool.

Parameter	Symbol	Value	Unit
Tool diameter	d_t	12	mm
Number of cutting edges	z_t	2	-
Clearance angle	α_f	12	°
Rake angle	γ_f	0	°
Helix angle	δ	0	°

The material specification includes autoclave curing of prepregs that combine HexPly 913 epoxy matrix and HTS carbon fibres in a $[0°]_{16}$ layup. The fibre volume content is

52 %. The material's thermal conductivity was experimentally determined and is provided in Table 2 for an ambient temperature of 28°C. Other properties are given according to [10] for the tested material.

Table 2. Material properties of the CFRP workpiece.

Parameter	Symbol	Value	Unit
Thermal conductivity in 1st orthotropic direction (parallel to fibres)	k_{11}	7.695	$\frac{\mathrm{W}}{\mathrm{m\cdot K}}$
Thermal conductivity in 2nd orthotropic direction (perpendicular to fibres)	k_{33}	0.630	$\frac{\mathrm{W}}{\mathrm{m\cdot K}}$
Specific heat capacity	C_p	879	$\mathrm{J/(kg\cdot K)}$
Density	ρ_w	1516	$\mathrm{kg/m^3}$
Fibre volume content	ϑ_{FVC}	52	%
Glass transition temperature	T_g	150.1	°C
Depth of cut (CFRP-panel thickness)	a_p	4.72	mm

2.2. Measurement equipment and process parameters

The experimental scheme is shown in Fig. 1. The peripheral milling tool processes the upper edge of a CFRP-panel to provide a straight horizontal cut. The tool feed rate is v_f. The length of cut l_m is 25 times the diameter of the cutting tool d_t. Testing was conducted with different fibre orientation angles Φ. This was achieved using rectangular workpiece panels, which were preliminary cut out with UD reinforcement aligned at specified angles to the upper side of the specimen. The tool interacting with the material is alternatively presented as a heat source of width s_{HS} and heat flux q_{HS}. Table 3 provides selected values for the setup arrangement.

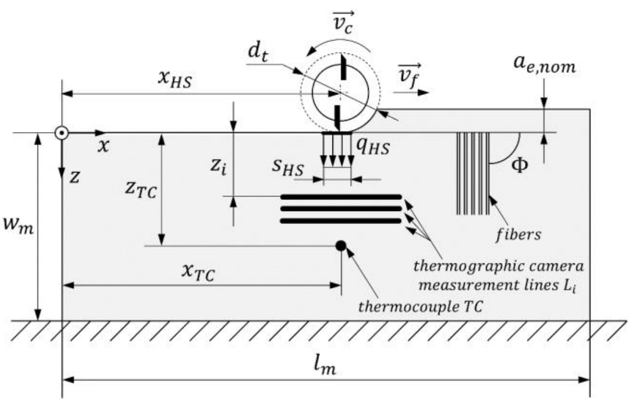

Fig. 1. Schematic representation of the machining situation of the CFRP-panels.

The cutting parameters were selected to comply with typical CFRP-trimming conditions in industrial production. Table 4 indicates the process parameters for the conducted tests. The length of the tool cutting edge along the tool axis was 22 mm. The thickness t of the tested CFRP-panels was equal to the depth of cut: $t = a_p$. This allowed for the use of three separate regions of the cutting edge, each approximately 7 mm in width. The cutting length processed by each cutting edge region was 1.5 m. The measured cutting-edge radius, which indicates tool wear, was less than r_β = 30 µm for the tested milling tools. Typically, it was close to 20 µm after the first 300 mm of machined path. Thus, the tool geometry can be assumed to be constant.

Table 3. Setup parameters for modeling and experiments.

Parameter	Symbol	Value	Unit
Length of machined path	l_m	300	mm
Distance in transversal direction from cutting surface to workpiece clamp	w_m	50	mm
Distances to the lines of measurement with the thermographic camera	z_i	0.7 / 0.92 / 1.38	mm
Horizontal distance to TC	x_{TC}	177.8	mm
Vertical distance from machined surface to TC	z_{TC}	1.5	mm
Nominal width of cut	$a_{e,nom}$	1.5 / 12	mm
Fibre orientation angle	Φ	22.5 / 45 / 67.5 / 90 / 112.5 / 135 / 157.5	°

Table 4. Investigated range of machining parameters for experiments and successive modeling.

Parameter	Symbol	Values in test series				Unit
Test series number		I	II	III	IV	
Cutting speed	v_c	100	100	450	450	$\frac{\mathrm{m}}{\mathrm{min}}$
Feed	f	0.06	0.1	0.06	0.1	mm
Feed rate	v_f	159	283	716	1273	$\frac{\mathrm{mm}}{\mathrm{min}}$

Fig. 2 illustrates the setup corresponding to the machining situation. The experiments were performed on a 5-axis machining center Reichenbacher VISION II-Sprint. Torque and corresponding mechanical processing power P_c were measured using a rotational 4-component dynamometer Kistler Typ 9170A with a signal conditioner Kistler Typ 5238B. The accuracy of torque measurement was 0.1 Nm.

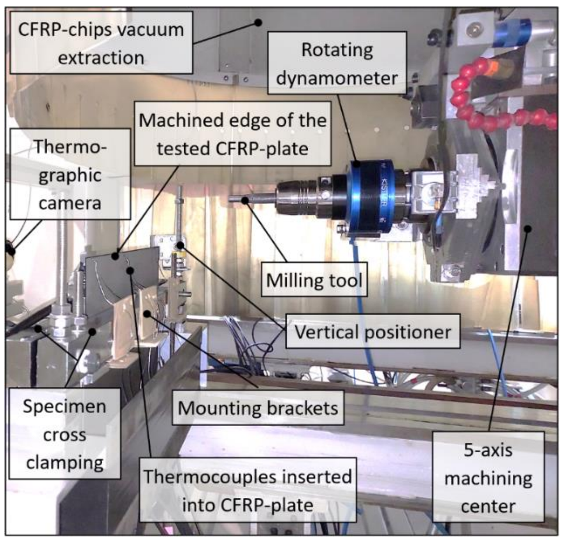

Fig. 2. Experimental setup, including thermocouples, thermographic camera, and rotating dynamometer.

The temperature data were obtained from the thermographic camera and the thermocouple. Multiple checks showed that the temperature deviation between measurements taken with both methods at the same points on the workpiece did not exceed 4°C or 3% of the measured value. This level of accuracy is consistent with the specifications of the devices used.

A shielded thermocouple of type J (Fe/CuNi) from TC Direct was inserted into the CFRP-panel at the positions indicated in Fig. 1. The thermocouple was placed at the closest safe distance to the machined surface to avoid damage during milling while remaining sensitive enough to provide reliable data for model calibration. The hot junction of the thermocouple was positioned in a hole with a diameter of 0.6 mm and a depth of 2 mm, and thermal conductive paste was applied to ensure proper contact with the CFRP panel.

The thermographic camera Micro-Epsilon Thermo IMAGER TIM VGA was used to capture the frontal surface of the CFRP plate. Measurements were conducted at distances z_i corresponding to the lines L_i shown in Fig. 1. The sensitivity of temperature measurements over time was limited by a noise equivalent temperature difference (NETD) parameter of 40 mK. The spatial and temporal camera resolution was 640 x 480 pixels at a rate of 32 Hz.

2.3. Analytical modeling

A previously developed analytical model for the temperature field in the machining of orthotropic composites with arbitrary fibre orientation was utilized [9]. This model provides a solution to the heat transfer equation for an orthotropic material where the principal direction of orthotropy aligns with the fibre reinforcement direction at a fibre orientation angle Φ. The model describes the temperature distribution resulting from the action of a moving strip source (MSS) in a steady state (SS):

$$\mathrm{T}_{MSS,\Phi,SS} = \frac{q_{HS}}{\pi\sqrt{k_{11}k_{33}}}\int_{x_n-s_{HS}/2}^{x_n+s_{HS}/2} exp\left(\frac{\rho_w C_p v_f}{2k_{11}k_{33}}\cdot\left[(k_{11} - k_{33})(\mathrm{S}\cos^2\Phi + z_n\sin\Phi\cdot\cos\Phi) - k_{11}\,\mathrm{S}\right]\right)\cdot \mathrm{K}_0\left\{\frac{\rho_w C_p v_f}{2k_{11}k_{33}}\left(k_{11} - (k_{11}-k_{33})\cos^2\Phi\right)^{1/2}\left[(k_{11}-k_{33})\cdot\left((z_n^2 - \mathrm{S}^2)\cdot\cos^2\Phi - 2z_n\mathrm{S}\cdot\sin\Phi\cdot\cos\Phi\right) + k_{11}\,\mathrm{S}^2 + k_{33}z_n^2\right]^{1/2}\right\}d\mathrm{S} \tag{1}$$

where q_{HS} and s_{HS} represent the equivalent heat flux and thermal contact length of the heat source respectively, v_f is the velocity of the moving heat source, which equals the feed rate. Coordinates correspond to the system shown in Fig. 1, where x_n and z_n denote the position of a point of interest for which the temperature is modeled, and x_{HS} indicates the horizontal position of the heat source's center. The integration variable is $\mathrm{S} = x_n - x_{HS}$. K_0 is the modified Bessel function of the second kind of order zero. Other variables are defined according to the parameters given in Table 4.

The analysis of the maximum temperature change $\Delta\mathrm{T}_{max}$ at the machined surface in milling for different fibre orientation angles Φ was enabled by using the analytical model in Eq. (1). The heat flow P_{HS}, which is relevant to the thermal damage of material, is calculated as follows

$$\mathrm{P}_{HS} = s_{HS}\cdot q_{HS}\cdot a_p. \tag{2}$$

The estimated heat source's thermal contact length s_{HS} and heat flux q_{HS} are calculated by solving a nonlinear least-squares problem to fit the model described in Eq. (1) to the experimentally measured average maximum temperatures. These temperatures are measured by the thermographic camera along each measurement line L_i at distances z_i as well as by the thermocouple at the distance z_{TC} from the machined surface. Ratio of heat flow to cutting power $\mathrm{R}_W = \mathrm{P}_{HS}/\mathrm{P}_c$ indicates the portion of the mechanical processing power P_c that is converted into heating of the machined surface.

3. Results and discussion

Simulated and measured maximum temperature changes $\Delta\mathrm{T}_{max}$ at the machined surface (MS) and at a small distance from it are presented in Fig. 3 for nominal full cut for various tested fibre orientation angles Φ. High values of maximum temperature change $\Delta\mathrm{T}_{max}$ at the machined surface in many experiments indicate an exceeding of the glass transition temperature T_g of the matrix both at lower (v_c = 100 m/min, Fig. 3, top) and higher (v_c = 450 m/min, Fig. 3, bottom) cutting speeds. Temperature changes above T_g lead to energy consumption for detrimental change of the material structure reducing further temperature increase. As the model doesn't capture this effect, as well as convection with the surrounding and heat radiation from the machined surface, its validity is limited for temperatures above T_g. Additional temperature measurements indicate that due to the before-mentioned effects the maximum temperature may occur slightly below the machined surface.

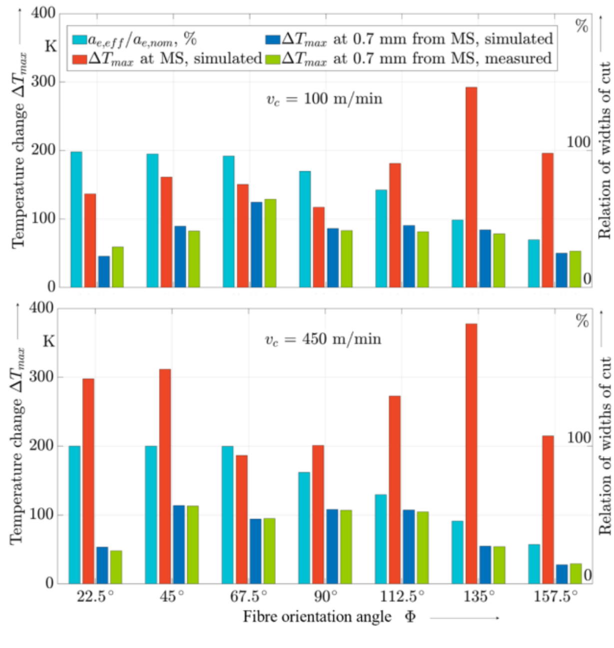

Fig. 3. Simulated maximum temperature change at the machined surface (MS), simulated and measured maximum temperature changes at a distance of z = 0.7 mm from the MS, and the ratio of effective to nominal widths of cut vs. fibre orientation angle Φ in milling at low (top) and high (bottom) cutting speeds with f = 0.06 mm and $a_{e,nom}$ = 12 mm.

Accordingly, the maximum temperature change $\Delta\mathrm{T}_{max}$ was simulated at a tested distance of z = 0.7 mm from the machined surface. This distance was chosen because it allowed reliable temperature measurement using the thermographic camera. At smaller distances from the machined surface or even on the MS, the tool and surrounding, which have different emissivity compared to the workpiece, can affect the accuracy of the thermographic measurements [6]. As it can be seen in Fig. 3, the simulated and measured maximum temperature changes $\Delta\mathrm{T}_{max}$ at the distance of z = 0.7 mm from the machined surface are closely aligned, with a mean deviation of 3°C.

Apart from the variation of v_c, the results are affected by break-outs of large-scale material particles due to up-cut milling leading to a reduced effective width of cut $a_{e,eff}$. This phenomenon was observed for several process parameters. It is described in detail below and indicated by the ratio of $a_{e,eff}/a_{e,nom}$. Higher cutting speed v_c results in an average temperature decrease of 10.5 % at the tested distance of z = 0.7 mm for different fibre orientation angles Φ. However, at the machined surface, simulated temperatures are significantly higher at higher v_c. This finding is in accordance with temperature measurements in down-cut milling of UD CFRP at lower cutting speeds [4]. Consequently, the heat-affected zone is much smaller at higher v_c, resulting in a steeper temperature gradient perpendicular to the machined surface. This effect is due to the increase in the velocity v_f of the moving heat source when milling at a constant feed f and varying v_c.

It can be observed in Fig. 3 that the minimum temperature gradient between the machined surface and points at the tested distance of z = 0.7 mm occurs at the fibre orientation angle Φ = 90°. This can be explained with an efficient heat transport from the contact zone perpendicular to the machined surface, as this direction aligns with the fibres providing much higher thermal conductivity k_{11} compared to k_{33} along the MS, i.e. perpendicular to the fibre direction. The deviation of the fibre direction from the surface normal can be expressed by the fibre orientation symmetry angle ζ_Φ. The more the fibre orientation angle Φ deviates from the angle of 90°, i.e. the higher is the fibre orientation symmetry angle ζ_Φ = Φ - 90° for Φ > 90° or ζ_Φ = 90° - Φ for Φ < 90°, the higher is the temperature gradient in the direction perpendicular to the machined surface. This can explain an approximate symmetry of dependencies of the maximum temperature changes ΔT_{max} relative to Φ = 90°.

The form of these dependencies is typical for the process parameters $v_c, f, a_{e,nom}$ in the test series as indicated in Tables 3 and 4. The test series show that the lower feed f results in a higher T_{max} under the same other conditions with an average temperature increase of 20.4 % at the tested distance for different fibre orientation angles Φ. Similarly, the higher nominal width of cut $a_{e,nom}$ leads to a higher T_{max} under the same other conditions with an average temperature increase of 15.8 % at the tested distance for different Φ.

For all the tested sets of process parameters $v_c, f, a_{e,nom}$, the highest maximum temperature T_{max} is observed for Φ = 135°. This statement applies regardless of whether the effective width of cut $a_{e,eff}$ is equal to the nominal one $a_{e,nom}$ or is significantly smaller. Similarly, the highest maximum temperatures T_{max} for Φ = 135° were also reported in [4] for down-cut milling of UD-CFRP at lower cutting speeds.

Dependencies of cutting power P_c on the fibre orientation angle Φ that are typical for the tested process parameters v_c, f for the two levels of $a_{e,nom}$ are shown in Fig. 4. P_c was calculated with the mean torque $M_{z,mean}$ from the measured torque $M_z(t)$ as illustrated in Fig. 5. At $a_{e,nom}$ = 1.5 mm the cutting power P_c exhibits a slightly parabolic dependency on the fibre orientation angle with a maximum in the angle range of 67.5° ≤ Φ ≤ 112.5°. The minimum cutting power always occurs at Φ = 22.5°. The maximum cutting power is 2 to 3 times the minimum value. At $a_{e,nom}$ = 12 mm, representing a full cut, there is a sharp decrease in cutting power with increasing fibre orientation angle Φ. However, this drop is primarily caused by the fact that the effective width of cut $a_{e,eff}$ drops drastically from the fibre orientation angle of Φ = 112.5° to Φ = 157.5° due to break-outs of large-scale material particles.

The break-out phenomenon, which typically occurs during a full cut, is compared with an undisturbed cutting process using in-process photos and torque curves over a single tooth engagement, as shown in Fig. 5. In general, the workpiece material must withstand the cutting force to ensure a stable machining process. In up-cut milling of UD-CFRP, this requirement is not met due to the low tensile strength perpendicular to the fibres when the cutting force is applied along an unfavorable direction [12], combined with a missing material support on the offcut side. Break-out is identified by a sudden drop in cutting torque over time. Since the engagement angle φ, fibre cutting angle θ and the current width of cut $a_e(\varphi)$ are dependent on time t, they can be calculated in the case of full cut ($a_{e,nom} = d_t$) as follows:

$$\varphi = 360° \cdot n\,t, \quad 0° \le \varphi \le 180°, \tag{3}$$

$$\theta = \Phi + \varphi, \tag{4}$$

$$a_e(\varphi) = \frac{d_t}{2}(1 - \cos\varphi). \tag{5}$$

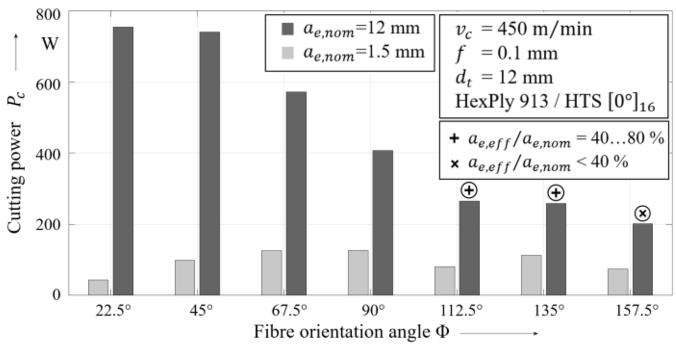

Fig. 4. Cutting power vs. fibre orientation angle Φ.

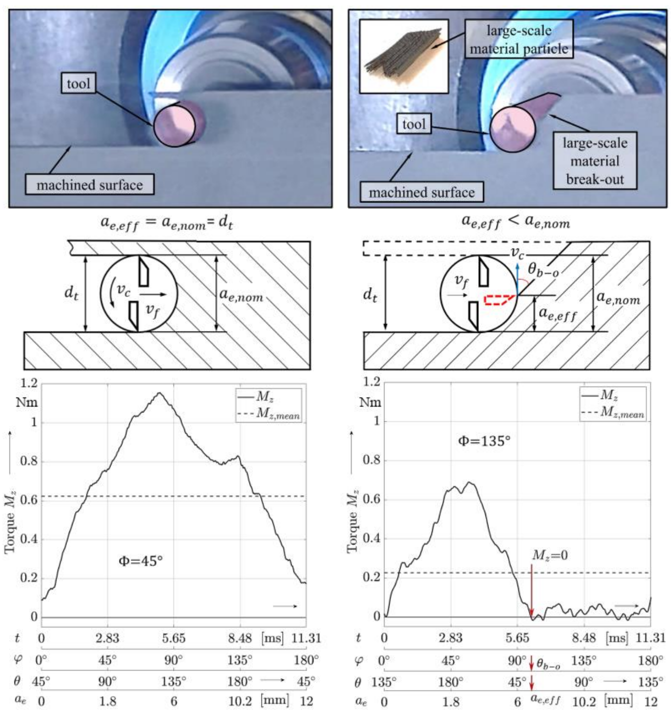

Fig. 5. Photos of the cutting process, diagrams of large-scale material break-out, and dependencies of torque M_z depending on time t, tool tooth engagement angle φ, fibre cutting angle θ, widths of cut a_e at fibre orientation angles Φ = 45° (left) and Φ = 135° (right).

Thus, the effective width of cut $a_{e,eff}$ and the fibre cutting angle at break-out θ_{b-o} are evaluated from the drop in cutting torque M_c for process parameters in full cut at $112.5° \leq \Phi \leq 157.5°$, where break-outs occur as illustrated in Fig. 5. It is found that the fibre cutting angles at break-out θ_{b-o} are within a narrow range of $39.8° \leq \theta_{b-o} \leq 50.1°$ regardless of the different $a_{e,eff}/a_{e,nom}$ for varying fibre orientation angles Φ, as it can be seen from the dependencies of θ_{b-o} on Φ shown in Fig. 6. The principal stresses due to shear for this range of θ_{b-o} correspond to the material compression along the fibres and tension perpendicularly to the fibres, representing the most unfavorable situation from the point of view of material strength [11].

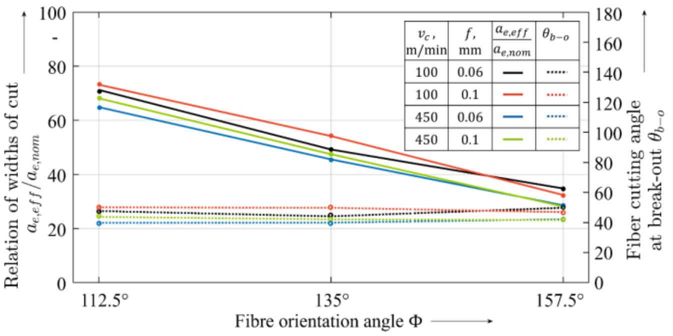

Fig. 6. The relationship of widths of cut $a_{e,eff}/a_{e,nom}$ and the fibre cutting angle θ_{b-o} at large-scale material break-out vs. fibre orientation angle Φ.

Parameters according to the analytical model given in Eq. (1) were identified using the Trust-Region-Reflective Least Squares Algorithm, as described in [9], based on the measured temperatures shown in Fig. 3. The results for heat flow P_{HS}, equivalent heat flux q_{HS} and thermal contact length s_{HS} are given in Fig. 7. It is evident that points with the same fibre orientation symmetry angles ζ_Φ exhibit similar thermal parameters s_{HS} and q_{HS} of the machining process. For each set of process parameters v_c, f and $a_{e,nom}$, higher fibre orientation symmetry angles ζ_Φ correspond to higher q_{HS} and lower s_{HS}, while lower ζ_Φ correspond to lower q_{HS} and higher s_{HS}. This result underscores that heat transport into the workpiece surface is primarily influenced by the deviation of the fibre direction from the surface normal. This is qualitatively illustrated by the ζ_Φ-curve. In addition, the heat transport is affected by different fibre orientation angles Φ with according material separation mechanisms and corresponding directions of movement of the strip-shaped heat source.

As can also be seen from Fig. 7, experiments involving large-scale material break-outs and correspondingly lower ratios of $a_{e,eff}/a_{e,nom}$ are characterized by lower s_{HS} compared to undisturbed tests at the same fibre orientation symmetry angles ζ_Φ and process parameter sets. Thus, the analytical model allows to capture the influence of large-scale material break-outs on heat transport into the workpiece surface.

A comparison of the results between large and small nominal width of cut $a_{e,nom}$ shows that, as expected, the heat flow P_{HS} is higher at the large nominal width of cut. According to Eq. (2), hyperbolas represent constant P_{HS} in Fig. 7. However, no clear trends can be identified for q_{HS} and s_{HS}. This is likely due to the simplified analytical model of the strip-shaped heat source, which neglects heat dissipation in regions distant from the machined surface, that are subsequently removed by following tooth engagements. Depending on the fibre orientation angle Φ and the nominal width of cut $a_{e,nom}$, heat can either be conducted into the leading material offcut or from it into the workpiece.

A comparison of the results between large and small feeds f shows that the heat flow P_{HS} is slightly higher at the large feed as indicated by the hyperbolas of constant P_{HS} in Fig. 7. Again, no clear trends can be identified regarding q_{HS} and s_{HS}.

The strong influence of v_c on P_{HS}, q_{HS} and s_{HS} is also evident from Fig. 7. Regardless of the parameter sets of fibre orientation angle Φ, nominal width of cut $a_{e,nom}$ and feed f, the corresponding combinations of q_{HS} and s_{HS} cluster into two groups based solely on the cutting speed v_c.

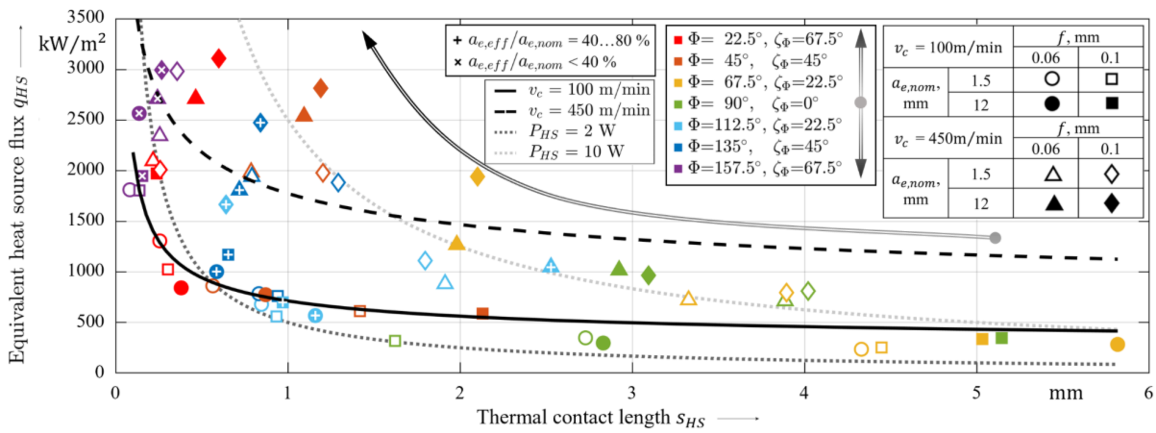

Fig. 7. Equivalent heat flux q_{HS} vs. thermal contact length s_{HS} at varying cutting speeds v_c, feeds f and nominal widths of cut $a_{e,nom}$. Relation $a_{e,eff}/a_{e,nom}$ =80…100 % if not additionally indicated.

Consequently, the corresponding points were empirically approximated using two balancing polynomials. As expected, the fitting curve for $v_c = 450$ m/min is shifted toward higher heat flows P_{HS} compared to the curve for $v_c = 100$ m/min.

From the fact that the fitting curves intersect with the hyperbolas of constant heat flow P_{HS}, it can be deduced that relatively lower heat flows occur to the left of the intersection point, i.e. in the direction of increasing orientation symmetry angles ζ_Φ. Conversely, relatively higher heat flows occur to the right of the intersection point, i.e. in the direction of decreasing orientation symmetry angles ζ_Φ.

By combining the measured cutting power P_c with the modeled heat flow P_{HS} as shown in Fig. 4 and 7, the ratio of heat flow to cutting power R_W can be calculated. R_W is primarily influenced by the nominal width of cut. For $a_{e,nom}$ = 1.5 mm R_W ranges from 5 % to 20 %. For $a_{e,nom}$ = 12 mm R_W amounts to 1.1 % ≤ R_W ≤ 7.4 %. These results align with expectations, as, in the case of a full cut, most of the generated heat is either carried away by the chips or conducted into the cutting surface of the leading material offcut that is currently being machined. The findings are consistent with previous results obtained for a low nominal width of cut [9].

4. Summary and outlook

The heat flow into the workpiece surface and the maximum temperature increase ΔT_{max} during up-cut milling of UD-CFRP were investigated experimentally and using an analytical model. The findings are summarized as follows.

The glass transition temperature T_g of the CFRP resin is exceeded under most of the tested cutting conditions.

Based on temperature measurements using thermocouples and a thermographic camera in the vicinity of the machined surface, thermal parameters s_{HS} and q_{HS} of the machining process were identified, and the maximum temperature increase ΔT_{max} was simulated, resulting in a mean deviation of 3°C from the measured ΔT_{max}.

Higher cutting velocities result in a smaller extension of the heat-affected zone but lead to a higher maximum temperature increase ΔT_{max} at the machined surface.

The highest maximum temperature increase occurs at the fibre orientation angle Φ = 135°.

The maximum temperature increase and thermal parameters of the machining process exhibit an approximate symmetry with regard to the fibre orientation angle Φ = 90°, when fibres are normal to the machined surface. Thus, the orientation symmetry angle ζ_Φ was introduced.

Break-out of large-scale material particles was observed in full cuts at Φ ≥ 112.5° due to up-cut milling, leading to reduced effective widths of cut $a_{e,eff}$. Break-outs occur at fibre cutting angles within a narrow range of θ_{b-o} near θ_{b-o} = 45° due to inter-fibre failure under transverse tension.

Simulated heat flow P_{HS}, equivalent heat flux q_{HS} and thermal contact length s_{HS} are highly dependent on fibre orientation symmetry angles ζ_Φ. Higher ζ_Φ leads to higher q_{HS}, lower s_{HS} and lower P_{HS}, and vice versa.

Higher cutting speeds v_c lead to higher heat flow P_{HS} at higher q_{HS}.

As a result of the study, the evaluated dependency of the model parameters on the cutting conditions allows to select favorable machining parameters avoiding critical material temperatures.

In the future, the influence of different tools and composite materials needs to be investigated, and the analytical model of the strip-shaped heat source should be extended to account for additional heat dissipation effects.

Acknowledgements

We would like to acknowledge and cordially thank the German Research Foundation DFG for funding support of the project 461768523 GZ: HI 843/14-1 AOBJ: 679098.

References

[1] Geier N, Xu J, Poór D, Dege J, Davim J. A review on advanced cutting tools and technologies for edge trimming of carbon fibre reinforced polymer (CFRP) composites. Composites Part B: Engineering 2023; 266: 111037. https://doi.org/10.1016/j.compositesb.2023.111037.

[2] Yashiro T, Ogawa T, Sasahara H. Temperature measurement of cutting tool and machined surface layer in milling of CFRP. Int. J. of Machine Tools and Manufacture 2013; 70:63-69. http://dx.doi.org/10.1016/j.ijmachtools.2013.03.009.

[3] Hintze W, Klingelhöller C. Analysis and modeling of heat flux into the tool in abrasive circular cutting of unidirectional CFRP. Procedia CIRP 2017; 66:210-214. https://doi.org/10.1016/j.procir.2017.03.305.

[4] Wang H, Sun J, Zhang D, Guo K, Li J. The effect of cutting temperature in milling of carbon fiber reinforced polymer composites. Composites Part A: Applied Science and Manufacturing 2016; 91:380-387. https://doi.org/10.1016/j.compositesa.2016.10.025.

[5] Karpat Y, Bahtiyar O, Deger B. Mechanistic force modeling for milling of unidirectional carbon fiber reinforced polymer laminates. Int. J. Machine Tools & Manufacture 2012; 56:79-93. https://doi:10.1016/j. ijmachtools. 2012.01.001.

[6] Sheikh-Ahmad JY, Almaskari F, Hafeez F. Thermal aspects in machining CFRPs: effect of cutter type and cutting parameters. Int J Adv Manuf Technol 2019; 100:2569-2582. https://doi.org/10.1007/s00170-018-2881-1.

[7] Sakkaki M, Moghanlou F, Vajdi M, Pishgar F, Shokouhimehr M, Asl M. The effect of thermal contact resistance on the temperature distribution in a WC made cutting tool. Ceramics Int 2019; 45(17A):22196-22202. https://doi.org/10.1016/j.ceramint.2019.07.241.

[8] Jaeger JC. Moving sources of heat and the temperature at sliding contacts. J and Proc of the Royal Soc of NSW 1942; 76: 203–224.

[9] Mehnen J, Hintze W, Köttner L, von Wenserski R. Temperature field due to a moving heat source in machining orthotropic composites with arbitrary fibre orientation. Procedia CIRP 2019; 85, 2-7. https://doi.org/10.1016/j.procir.2019.09.019.

[10] Mehnen J, Modellgestützte Berechnung der thermischen Belastung bei der Zerspanung von unidirektionalem CFK, Dissertation, TU Hamburg, 2023.

[11] Düreth C, Weck D, Böhm R, Thieme M, Gude M, Henkel S, Wolf CH, Biermann H. Determining the damage and failure behaviour of textile reinforced composites under combined in-plane and out-of-plane loading. Materials 2020; 13(21):4772-45. https://doi.org/10.3390/ma13214772.

[12] Brouschkin A, Hintze W, Dege JH. Influence of spatial engagement angles on machining forces and surface roughness in turning of unidirectional CFRP. CIRP JMST 2024; 51:201-203. https://doi.org/10.1016/j.cirpj.2024.03.010.